Structure of submonolayer gold on silicon (111) from x-ray standing-wave triangulation

Lonny E. Berman* and Boris W. Batterman
School of Applied and Engineering Physics and the Cornell High Energy Synchrotron Source (CHESS), Cornell University, Ithaca, New York 14853

Jack M. Blakely
Department of Materials Science and Engineering, Cornell University, Ithaca, New York 14853
(Received 4 April 1988)

The three-dimensional registry of a submonolayer Au film adsorbed on a Si(111) surface was measured using the x-ray standing-wave method. Au photoelectron yields were monitored as the (111), (220), and (11$\bar{1}$) reflections from the substrate were scanned. These results were combined with symmetry considerations in order to triangulate the Au position relative to the bulk crystal structure. An unusual adsorption site, one which is embedded in the substrate and bridges two Si atoms in the lower half of the (111) double layer, agrees well with the data.

I. INTRODUCTION

The Au/Si interface has been the subject of extensive investigation because of its use in semiconductor-device technology.[1] At Au coverages exceeding ~ 3 monolayers (ML), interdiffusion occurs at room temperature, leading to a film of complex structure which has a diffuse interface with the substrate and is capped with a mixed Au/Si surface layer.[2-4] At high temperature (>400 °C), Au-film growth follows the Stranski-Krastanov mechanism, in which islands of Au agglomerate on top of a surface monolayer;[5,6] the islands are believed to be covered by a mixed, reacted Au/Si skin.[7] Less is known of the structure of the Au/Si(111) interface in the monolayer Au coverage range. Ordered superstructures for annealed interfaces have been identified through low-energy electron diffraction[8,9] (LEED) and correlated with Au coverage using Auger-electron spectroscopy (AES).[10] Recent electron-diffraction and microscopy,[11,12] low-energy ion-scattering,[13,14] and scanning-tunneling-microscopy[15] measurements have provided more information on the atomic structures of these Au superlattices. Ion-scattering data for a surface covered with 0.3 ML of Au, exhibiting a (5×1) reconstruction,[9,10] were consistent with a model in which the Au atoms embedded below one Si atom layer.[13] From ion-scattering data for a surface with a higher Au coverage, which exhibited a $(\sqrt{3}\times\sqrt{3}R30°)$ superlattice,[9,10] it was concluded that the Au atoms clustered into triplets above the surface.[14]

In this paper we report results of x-ray standing-wave measurements on a 0.35-ML Au film adsorbed on a Si(111) surface in ultrahigh vacuum (UHV). Au photoelectron yields were monitored as the (111), (220), and (11$\bar{1}$) Bragg reflections from the substrate were scanned. These results, and symmetry considerations, enable us to triangulate the Au-atom position relative to the bulk Si atomic positions. These data constitute an extension of results we previously reported using the (111) reflection, which identified the coordinate of the Au atoms normal to the (111) diffraction planes.[16] Since the (220) and (11$\bar{1}$) diffraction planes are inclined relative to the Si(111) surface, the new data also provide information on the coordinates of the Au atoms *in* the (111) planes.

The x-ray standing-wave method of atom location[17,18] has been applied in several investigations of bulk and surface structures. When a perfect crystal is oriented to excite a Bragg reflection, the incident and diffracted x-ray beams interfere to produce a wave traveling along the diffraction planes with nodal and antinodal planes parallel to the diffraction planes.[19,20] The total wave is usually referred to as a standing wave. In the Bragg diffraction geometry (in which the entrance and exit beams pass through the same surface), the standing-wave nodes move continuously from the diffraction planes to between the planes as the incidence angle is scanned through the reflection; the nodes move inward by half a d spacing with respect to the planes as the angle is advanced. By monitoring fluorescence, Auger, or photoelectron yields from particular types of atoms in the crystal, as the standing-wave field is moved, the positions of these atoms relative to the diffraction planes can be determined. The standing-wave field extends beyond the surface, so that atomic positions can be determined even in distorted surface regions[21-24] and overlayers.[25] Such measurements have pinpointed atomic positions to better than 10^{-2} of a d spacing.

Batterman[18] first determined the location of a bulk impurity from standing-wave measurements using symmetric Bragg reflections from samples of different orientation. Golovchenko *et al.*[26] later demonstrated that three-dimensional positional coordinates of a surface adsorbate could be determined by combining results from measurements on one sample using nonparallel diffraction planes. Similar triangulation studies have been performed by others.[27-29] The data presented in this paper were collected using diffraction from the (111), (220), and (11$\bar{1}$) sets of Bragg planes of a Si(111) sample.

II. EXPERIMENTAL PROCEDURE

The measurements were performed at the Cornell High Energy Synchrotron Source (CHESS) in the B-Cave station, with the same experimental setup used in our previous work.[16] The variable-angular-resolution monochromator optics[30,31] and some aspects of the UHV chamber[16] have been described. For this particular experiment, four bounce Si(111) and Si(220) channel-cut crystal monochromators[31] were used for the {111} and (220) reflection standing-wave measurements, respectively. The sample was positioned at the focus of a double-pass cylindrical mirror analyzer[32] (CMA) for the measurements. The locations of the entrance and exit beryllium windows on the chamber constrained the scattering plane to be horizontal. Hence, the UHV sample holder was outfitted with special goniometry to allow the (111), (220), and $(11\bar{1})$ reflections to be rotated into a symmetric scattering geometry in the horizontal plane while maintaining the sample at the CMA focus. The base pressure of the chamber was 1.5×10^{-10} Torr during the measurements.

A Si(111) sample was fabricated from float-zone–refined stock, Syton polished, and chemically treated using Henderson's method[33] prior to insertion in the UHV chamber. This treatment involves the growth of a nearly carbon-free surface oxide layer, which will volatilize in UHV when heated to $\simeq$900 °C.[33] A short flash to $\simeq$1200 °C is then required to remove the residual carbon contamination. Our samples have consistently been found to be clean to within the detectability limit of our Auger spectrometer (1% of a monolayer of impurities) following this treatment, and give sharp (7×7) LEED patterns. Sample annealing was accomplished using tantalum "hot heaters."[34]

An unfortunate side effect of heating the sample to 1200 °C is plastic deformation. In this and our previously reported UHV standing-wave measurements,[16,35] plastic deformation often resulted in observed sample reflectivity curves which were distorted in comparison with those from control samples in open-air bench tests[31] and from unheated samples mounted in our UHV chamber. We carefully characterized the deformation in the sample used for this work through x-ray reflectivity, x-ray topography, and etch-pit profiling; these showed that slip induced by thermal stress[36] caused it to become concave, with a radius of curvature of $\simeq$700 m. Although enormous, this radius was still small enough to significantly distort the reflectivity curves, which themselves were just a few arcsec wide. An important conclusion of these characterizations was that the sample strain fields were sufficiently long ranged that they would not prevent the formation of the standing wave. In fitting theory to the observed reflectivity data, we have included corrections for sample distortion since the area of the surface sampled in the measurements (a few mm^2) was large enough to introduce systematic perturbations of the expected curves. The thermal-stress-induced distortion becomes significant for annealing temperatures higher than 1000 °C. Future standing-wave work on Si should use the recently developed low-temperature cleaning procedure of Ishizaka and Shiraki,[37] which has already been used successfully in UHV standing-wave experiments.[38–40]

After preparing a clean surface showing a sharp (7×7) LEED pattern, 0.35 ML of Au (Ref. 41) was deposited onto the surface at room temperature from an evaporation cell. This resulted in a (1×1) LEED pattern with a high background. A first set of standing-wave measurements was performed for this surface. The sample was then annealed at 650 °C to produce a sharp (5×1) LEED pattern. A second set of measurements was then performed, followed by a third set of measurements [except for the (220) reflection] a day later without disturbing the sample. Each set of data was collected over the course of a day. After the final set, the LEED pattern was still observed to be (5×1). The third set of measurements was made primarily to observe the effect of surface contamination from the residual gas background on the data, since small carbon and oxygen Auger peaks were found to build up over the duration of the experiment.

The data-collection procedure was similar to that used in our earlier work.[16] The sample Bragg angle for the appropriate reflection was set to diffract an x-ray energy which was 1700–1800 eV above a Au L absorption edge, producing a sharp Au L photoelectron peak in the CMA spectrum, in a region of relatively low background (i.e., beyond the Si Auger peaks). The CMA window (energy width of 30 eV) was tuned to the Au photoelectron peak, and a first set of data was collected by monitoring the photoelectron yield as the sample reflectivity curve was scanned. This was accomplished by scanning the monochromator angle while leaving the sample fixed. To remove the background contribution to the observed CMA output, another set of data was collected after lowering the x-ray energy enough to move the Au L photoelectron peak below the fixed CMA window. The difference of the two sets represents the net Au L photoelectron standing-wave yield. This procedure guarantees that the net yield is produced solely by x-ray excitation, an advantage not realized when monitoring features of fixed energy due to Auger and fluorescence transitions.

Au $L_{\rm III}$ photoelectron yields were monitored for the (111) and $(11\bar{1})$ reflections, and $L_{\rm II}$ yields were monitored for the (220) reflection. The nominal x-ray energies were 13.7 keV for the {111} reflections and 15.5 keV for the (220) reflection. For the {111} reflections the angular width of the beam transmitted by the monochromator was set to approximately one-quarter of the sample Darwin reflectivity width[42] [the case corresponding to Fig. 5(d) of Ref. 31]. For the (220) reflection the transmitted width was set to approximately one-half of the Darwin width [corresponding to Fig. 5(c) of Ref. 31].

III. MODEL-INDEPENDENT DIFFRACTION ANALYSIS

The data are presented in Fig. 1 for (a) the (1×1) (Au as-deposited), (b) the fresh (5×1) (annealed), and (c) the day-old (5×1) surfaces. For each reflection the lowest curve is the reflectivity and the upper ones represent the appropriate Au emission yield, normalized to unity away from the Bragg reflection. The solid lines are fits to the

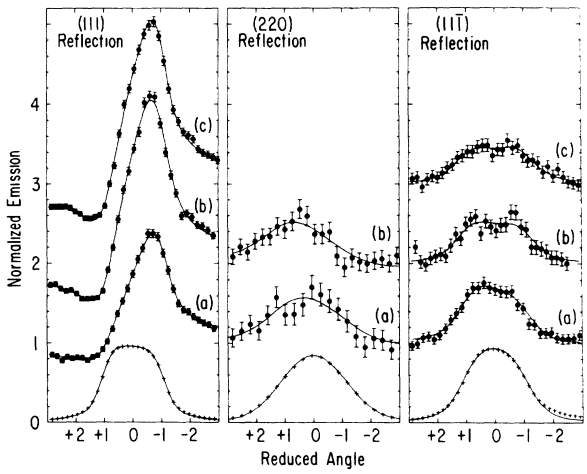

FIG. 1. Au photoelectron standing-wave yields are shown for (a) the (1×1) (Au as-deposited), (b) the fresh (5×1) (annealed), and (c) the day-old (5×1) surfaces, using the (111) (left), (220) (middle), and (11$\bar{1}$) (right) reflections. Curves (b) and (c) are successively displaced by one unit along the ordinate. The lowest curves are the measured reflectivities and the solid lines are fits using dynamical theory. The reduced angle interval between $+1$ and -1 corresponds to the appropriate Darwin angular width [3.8 arcsec for the {111} reflections and 2.2 arcsec for the (220) reflection]; decreasing reduced angle means increasing x-ray energy.

data. The average net Au photoelectron count rates away from the Bragg condition were $\simeq 50$ sec^{-1} for the (111) reflection, $\simeq 2$ sec^{-1} for the (220) reflection, and $\simeq 8$ sec^{-1} for the (11$\bar{1}$) reflection, at incident photon fluxes of $\simeq 1\times10^{9}$, $\simeq 2\times10^{8}$, and $\simeq 5\times10^{8}$ sec^{-1}, respectively.

The photoelectron yield from a single Au atom would have a strong modulation as the reflection is scanned, simply representing the electric-field–intensity variation at its position. If the collection of Au atoms assumes not one but several positions relative to a set of diffraction planes, the emission yield is expected to have a much weaker modulation, representing an average of several phases of the standing-wave field. The strong variations for the (111)-reflection data sets [particularly the (5×1) surface sets] suggest that a large fraction of the Au atoms took on a unique position relative to the (111) planes, i.e., along the surface normal. Since the highest Au emission is close to the high-angle side of the (111) reflection, the preferred position must be close to the (111) diffraction plane, since the standing-wave–field antinode converges toward the diffraction plane on the high-angle side of the reflection. It is evident that more than one position with respect to the inclined (220) and (1$\bar{1}$1) planes was taken up by the Au atoms, for all surface conditions. This means that the Au atoms occupied more than one adsorption site in a surface (1×1) unit cell.

The reflectivity curves were fitted by convoluting the instrumental resolution function with the intrinsic Darwin-Prins reflectivity curve.[42,43] The determination of the resolution function, as well as the absolute angular reference and calibration for the yield data, establish the amplitude and phase of the experimentally produced standing wave. The resolution function itself consists of the convolution of the monochromator transmission function[31] with a function which accounts for the deformation profile of the sample.[44] A Gaussian function was used for the latter, with a determined 2σ width of 0.6 arcsec for the (111) reflection and 1.5 arcsec for both the (220) and (11$\bar{1}$) reflections. The (220) and (11$\bar{1}$) reflectivity curves appear more rounded than the (111) curve due to different contributions to the resolution function from the strain field.

In fitting the photoelectron-yield data, the standing-wave yield, given by[45]

$$Y(\theta)=Y_{oB}\left\{1+C_1\left|\frac{E_H}{E_0}[\theta]\right|^2 +2C_2\left|\frac{E_H}{E_0}[\theta]\right| f\cos(v[\theta]-2\pi\Phi)\right\}, \quad (1)$$

was convoluted with the resolution function and compared with the data for a best fit using a least-squares technique. E_0 and E_H are the (complex) incident- and diffracted-beam electric fields, respectively. $v(\theta)$ is the phase of E_H relative to E_0, and also represents the position of the standing-wave antinodes relative to the diffraction planes, with a suitable choice of unit-cell origin.[46,47] The C_1 and C_2 coefficients can be determined from dynamical diffraction theory[19,20] if the photoelectron yield is proportional to the electric field intensity at the center of the absorbing atom;[48] C_1 is unity and C_2 is a polarization factor, unity for the σ- or TE-polarization geometry, and $\cos2\theta_B$ (where θ_B is the nominal Bragg angle) for the π or TM geometry (used in our measurements).[49] Y_{oB} is the emission yield away from the Bragg reflection. f and Φ are usually referred to as the coherent fraction and coherent position,[45] respectively. They represent, respectively, the amplitude and $1/2\pi$ times the phase of the Fourier component of the Au-atom distribution relative to the diffraction planes.[50] Extinction effects have been ignored in Eq. (1), since the detected photoelectrons emanated from surface Au atoms. The parameters which were varied for a best fit to the data were Y_{oB}, f, and Φ.

The coherent position is a weighted average position of the Au atoms relative to the diffraction planes. It takes on a value between $-\frac{1}{2}$ and $+\frac{1}{2}$, with a value of 0 corresponding to a position on the planes, and $\pm\frac{1}{2}$ corresponding to a position midway between the planes. The coherent fraction is related to the spread of Au-atom positions. A value of 1 means that all the atoms are located at the same (coherent) position, and a value smaller than 1 means that they take on more than one position relative to the planes. It is the simple and direct extraction of phase as well as amplitude information which makes the standing-wave method powerful.

Table I lists the coherent position Φ and coherent fraction, f, values for the data shown in Fig. 1. The (111)-reflection data for the fresh and day-old (5×1) surfaces

TABLE I. Values for the coherent position, Φ, and coherent fraction, f, are presented for the data shown in Fig. 1.

Surf.	Refl.	Φ	f
(1×1)	(111)	−0.01±0.01	0.52±0.01
	(220)	−0.32±0.04	0.23±0.07
	(11$\bar{1}$)	−0.31±0.04	0.14±0.05
fresh (5×1)	(111)	+0.05±0.01	0.89±0.02
	(220)	−0.34±0.02	0.36±0.05
	(11$\bar{1}$)	−0.25±0.02	0.25±0.05
day-old (5×1)	(111)	+0.04±0.01	0.86±0.02
	(11$\bar{1}$)	−0.24±0.01	0.28±0.05

have high coherent fractions, consistent with the observed strong yield modulations. Since the coherent fraction was near unity, it can be concluded, without any detailed modeling, that the Au atoms were clustered around a position 0.15±0.03 Å above the (111) diffraction plane, along the surface normal for the fresh (5×1) surface. This agrees within experimental error with our previous results.[16] The (220) and (11$\bar{1}$) data have low coherent fractions, indicating that the Au atoms occupied more than one position relative to these inclined diffraction planes. The major differences between the (1×1) and (5×1) surface data are relatively large coherent fraction increases for all of the reflections, suggesting more order in the Au overlayer for the (5×1) surface. Finally, the fresh and day-old (5×1) surface data are in agreement within experimental error, indicating that the effect of surface contamination from the residual gas background on the data was not important.

IV. GOLD-ATOM LOCATIONS

The following analysis will concentrate on the fresh (5×1) surface. Two classes of adsorption, "embedded" (Au penetrating into the substrate) and "atop" (Au sitting above the surface), can be tested for consistency with the data. For the embedded case the Au atoms "sit" within a Si double layer at 5% of a (111) interplanar spacing above the (111) diffraction plane, which is the midplane of the double layer. For the atop case the preferred Au height corresponds to a position 105% of a (111) interplanar spacing above the last (111) diffraction plane in the bulk [i.e., 5% of a (111) spacing above the first (111) plane in the vacuum]. A (111)-reflection standing-wave measurement cannot distinguish between these two cases. To account for the measured (111) coherent-fraction value of 0.89, we will assume that 10% of the Au atoms are randomly distributed normal to the (111) planes, and use a (111)-reflection Au-overlayer Debye-Waller factor of 0.99 determined from LEED data on the (5×1) surface[51] to account for thermal vibrations.[52] The product of the "commensurate" fraction[53] of 0.90 with the Debye-Waller factor gives the coherent fraction.

The coherent fractions for the (220) and (11$\bar{1}$) data are much lower than that for the (111) data. The sharp LEED patterns and the trends observed with sample annealing indicate that these low values are more likely to be due to a multiplicity of preferred sites than to randomness in the distributions along the normals to these inclined planes. We will assume the random fraction to be 10% for the (220) and (11$\bar{1}$) distributions, as for the (111) case.

Figure 2 shows side and top views of the Si-atom positions within a surface (1×1) unit cell appropriate to the embedded adsorption case. The plane of the cell is at the Au-atom height, just above a (111) diffraction plane that is inside the bulk. The corresponding views for the atop case are shown in Fig. 3, in which the plane of the cell is just above the first (111) diffraction plane in the vacuum. The atop cell is shifted laterally by a {112} interplanar spacing relative to the embedded cell. If the stacking of Si atoms is continued into another double layer in Fig. 3, they would project into the plane of the unit cell as in Fig. 2.

A candidate adsorption site "1" is represented by polar coordinates r and θ relative to the centers of the unit cells in Figs. 2 and 3. If the Si substrate is ideally terminated with threefold rotational symmetry about the surface normal, and one type of bonding configuration between the Au atom and the substrate dominates, the sites labeled 2 and 3 will be equivalent to site 1 in Figs. 2 and 3. Sites 4–6 would also be equivalent due to the mirror symmetries about the {110} planes that are perpendicular to the surface, so that the (220) and (11$\bar{1}$) standing-wave yields should average over six equivalent positions. Naturally, steric hindrance would preclude the occupation of

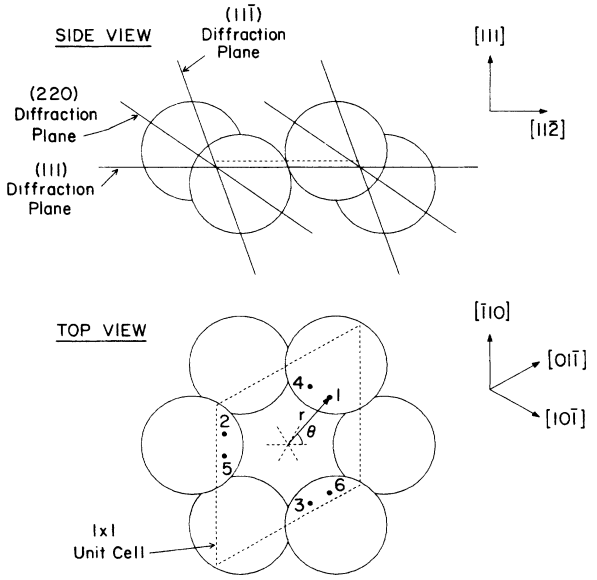

FIG. 2. Side and top views of an ideal Si(111) double layer for the embedded adsorption case. The Au atoms adsorb within a surface (1×1) unit cell (dashed) at a height of 5% of a (111) interplanar spacing above the (111) diffraction plane, which is the midplane of the double layer. A candidate adsorption site "1" has polar coordinates r and θ relative to the unit-cell center. Sites 2–6 are equivalent to site 1 due to the symmetries of the (111) surface.

more than one of these sites by Au atoms within any one unit cell.

The (220) and (11$\bar{1}$) standing-wave yields from the Au atoms were computed for different values of the coordinates r and θ. The ranges of coordinates which resulted in (220) and (11$\bar{1}$) coherent-position and coherent-fraction values that fall within the error bars of the measured ones are represented by filled patches in Figs. 4(a) and 4(b) for the embedded and atop cases, respectively. The (220) and (11$\bar{1}$) patches, though not overlapping, are very close to each other, and closely surround the midpoints of imaginary "bridge" lines which connect two second-layer Si atoms for the embedded case [Fig. 4(a)] and two first-layer Si atoms for the atop case [Fig. 4(b)]. We therefore conclude that these bridge sites are the most likely adsorption sites. The absence of any Au-atom density at or near the projected Si-atom positions, or at the centers of the hollows, seems to eliminate the substitutional, embedded sixfold hollow center, and the onefold- and threefold-coordinated atop sites. The substitutional site has been found for As.[40] The embedded sixfold hollow site has been identified for Ag,[54] Ni,[55] Cu,[56] and Pt,[57] and also suggested for Au.[13] Br,[26] I,[58] and Cl (Ref. 59) are believed to occupy the singly coordinated atop site.

Figure 5 shows the calculated standing-wave yields for the (220) and (11$\bar{1}$) reflections, from (a) Au atoms embed-

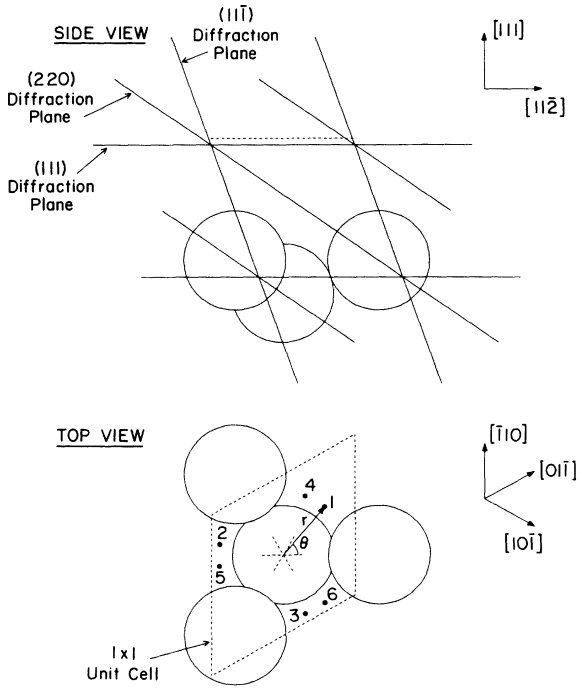

FIG. 3. Side and top views of the first Si(111) double layer for the atop adsorption case. The Au atoms adsorb within a surface (1×1) unit cell (dashed) at a height of 5% of a (111) interplanar spacing above the first (111) diffraction plane in the vacuum. The Si atoms project into the atop cell differently from the embedded cell of Fig. 2, since the former is laterally shifted by a {112} interplanar spacing relative to the latter.

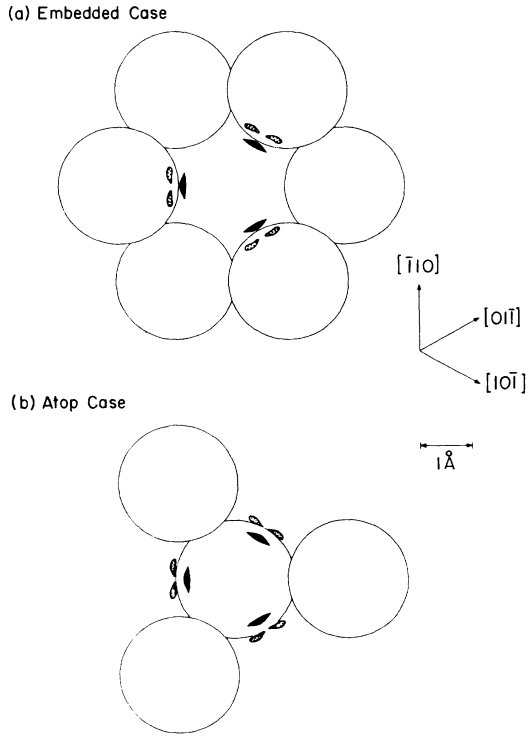

FIG. 4. The filled patches indicate the ranges of Au adsorption sites for (a) the embedded case and (b) the atop case. The black patches are consistent with the (220)-reflection data for the fresh (5×1) surface and the dotted patches are consistent with the (11$\bar{1}$) data.

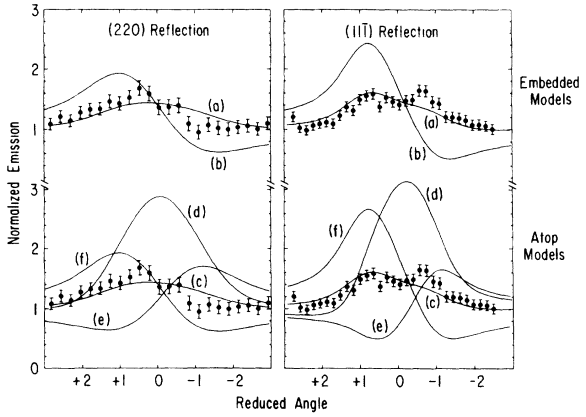

FIG. 5. The calculated photoelectron yields from Au atoms embedded at (a) sites which bridge two second-layer Si atoms and (b) hollow center sites, and atop the surface at (c) twofold-coordinated sites, (d) onefold-coordinated sites, (e) threefold-coordinated sites above the hollow, and (f) threefold-coordinated sites above a second-layer atom, are compared with the fresh (5×1)-surface (220)-reflection data (left) and (11$\bar{1}$) data (right).

ded at sites which bridge two second-layer Si atoms, and (b) Au atoms embedded at hollow center sites. Also shown are the corresponding yields for the atop adsorption case, with Au atoms situated at (c) the twofold-coordinated sites, (d) the onefold-coordinated sites, (e) the threefold-coordinated sites above the hollow, and (f) the threefold-coordinated sites above a second-layer Si atom. The quality of the fit to the experimental data may be characterized by the reduced χ^2, i.e., χ^2_ν.[60] $\chi^2_\nu \simeq 1$ for a fit which is considered to be good. Table II lists the coherent position Φ, coherent fraction f, and χ^2_ν values for the calculated yield curves shown in Fig. 5, as well as for the fitted data shown in Fig. 1. Only for the embedded and twofold atop bridge sites are the χ^2_ν values in the neighborhood of unity.

The analysis was repeated using different assumed values between 0% and 50% for the Au random fractions relative to the (220) and (11$\bar{1}$) planes. The effect of modeling the Au-atom distribution normal to the surface with a Gaussian function [of 2σ width equal to 14% of a (111) d spacing] rather than assuming any random fraction was also explored. Neither of these modifications changed the conclusions as to the most likely Au adsorption sites.

V. DISCUSSION

Possible arrangements of adsorbed Au atoms forming embedded and atop (5×1) overlayers which are consistent with the standing-wave data are shown in Figs. 6 and 7, respectively; they each represent one of three equivalent domains. Other arrangements consistent with the data in which the Au atoms take on the remaining bridge sites within a (5×1) unit mesh can be suggested, and could be tested via analyses of LEED and glancing-incidence x-ray-diffraction intensities. The Au-overlayer meshes shown in Figs. 6 and 7 have been suggested from LEED and AES data.[10] The standing-wave data provide information on the registries of these meshes relative to an ideal substrate, and therefore complement the symmetry information available from LEED.

The models involve no assumptions about relaxations of the substrate atoms. However, for the model shown in Fig. 6 the unrelaxed substrate would have first-layer Si atoms (not shown in the model) only 1.1 Å from the Au atoms and second-layer Si atoms at 2.0 Å. Since the bulk Si—Si and Au—Au bond lengths are 2.35 and 2.88 Å, respectively, some substrate rearrangement must take place. Certainly the first-layer Si atoms omitted from Fig. 6, if present, must undergo substantial displacements. For the twofold-coordinated atop model shown in Fig. 7, the Au—Si bond length would be 3.5 Å without substrate relaxation. Since this seems to be too large, at least part of the first Si layer would have to be relaxed. Si relaxations were not determined in our experiment, since the standing-wave measurements refer the Au position to an extrapolation of the bulk diffraction planes.

The embedded adsorption model of Fig. 6 is of the "interstitial" type proposed by Tu,[61] in which Si—Si bonds are weakened due to charge transfer to bonds with Au atoms which had diffused into interstitial sites in the substrate. Recent electron-spectroscopy measurements[62–65] seem to support the interstitial model.

The Au atoms shown in Fig. 6 need not be embedded in the first Si double layer for agreement with the standing-wave data. Embedding in deeper double layers would also be consistent. However, recent low-energy ion-scattering data from the (5×1) surface indicated that the Au submonolayer was shadowed by only one Si atom

TABLE II. Values for the (220) and (11$\bar{1}$) coherent position, Φ, coherent fraction, f, and χ^2_ν are presented for the emission-yield curves (Fig. 5) from Au atoms adsorbed at various embedded and atop sites. The corresponding values for the fitted data from the fresh (5×1) surface (Fig. 1) are shown for comparison.

Au adsorption site	(220) reflection Φ	f	χ^2_ν
(a) embedded bridge	−0.27	0.29	1.4
(b) embedded sixfold hollow	−0.44	0.87	8.8
(c) twofold atop	−0.27	0.29	1.4
(d) onefold atop	+0.23	0.87	11.3
(e) threefold atop a hollow	−0.10	0.87	22.9
(f) threefold atop a second-layer atom	−0.44	0.87	8.8
Fresh (5×1) surface data	−0.34±0.02	0.36±0.05	0.7
Au adsorption site	(11$\bar{1}$) reflection Φ	f	χ^2_ν
(a) embedded bridge	−0.32	0.30	1.9
(b) embedded sixfold hollow	−0.48	0.89	37.0
(c) twofold atop	−0.32	0.30	1.9
(d) onefold atop	+0.18	0.89	22.0
(e) threefold atop a hollow	−0.15	0.89	38.3
(f) threefold atop a second-layer atom	−0.48	0.89	37.0
Fresh (5×1) surface data	−0.25±0.02	0.25±0.05	0.8

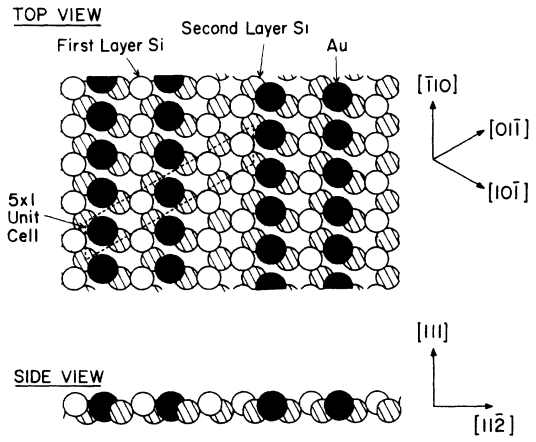

FIG. 6. Top and side views of one domain of an embedded Au overlayer that is consistent with the fresh (5×1) surface standing-wave data. The Au coverage is assumed to be 0.4 ML, slightly higher than the actual coverage in the measurements. The first-layer Si atoms, which would be less than 2 Å from the Au atoms in an unrelaxed substrate, are not included; otherwise, the Si atoms are shown at bulklike positions.

layer,[13] making the first double layer the preferred choice. The centers of the open surface hollows were specified as the adsorption sites,[13] instead of the lower-symmetry displaced sites suggested here. More recent high-energy proton-scattering data from an annealed Si(111) surface covered with 0.7 ML of Au (Ref. 66) agreed with the low-energy ion-scattering data.[13]

The atop adsorption model of Fig. 7 is of the type proposed by Hiraki,[67–70] but is not consistent with the low-energy ion-scattering results.[13] This unusual twofold coordination has been identified for Te adsorbed on Si(111),[58] but is not expected for Au, which shows monovalent and trivalent oxidation states.[71]

A potentially serious complicating factor in the analysis of the standing-wave data is the presence of a stacking fault in the (111) surface. While there appears to be no evidence that the first-layer stacking fault of the clean (7×7) reconstructed Si(111) surface[72,73] survives Au deposition,[74] we have nevertheless carefully studied how such a fault would complicate the interpretation of the standing-wave data. A complete stacking fault in the first Si layer causes the atoms in this layer to exchange positions with the open surface hollows. This would not affect the conclusions about nearest-neighbor coordination for the ideal-surface-embedded model shown in Fig. 6, since the second-layer arrangement is unaffected by the first-layer fault. However, for the atop model shown in Fig. 7, the locations determined for the Au atoms would not be sites of high symmetry relative to the topmost Si layer. These conclusions would not be altered if the first-layer stacking fault covers half the surface, as for the clean (7×7) surface.[73]

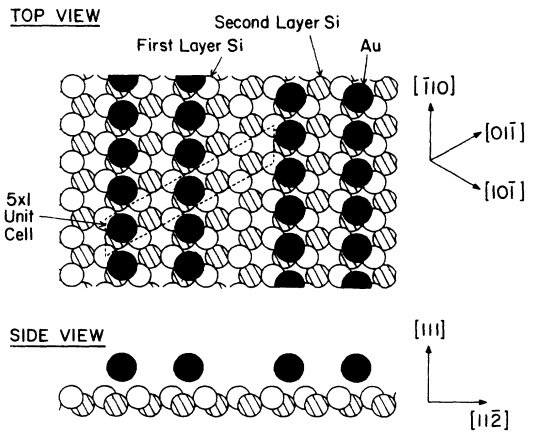

FIG. 7. Top and side views of one domain of an atop Au overlayer, which is consistent with the fresh (5×1)-surface standing-wave data. The Au coverage is assumed to be 0.4 ML.

It is clear that complementary measurements of the Au—Si bond length using the surface extended x-ray-absorption fine-structure (EXAFS) method[54,55,57–59] and quantitative diffraction studies would be very helpful in pinpointing relaxations of the Si surface layer. We considered performing standing-wave measurements on the Au-covered surface using the low-energy Si *LVV* Auger channel to achieve Si surface sensitivity,[35] as in our previous measurement.[16] Recent work, however, has shown that the determination of the positions of Si atoms in the surface layer using this particular yield channel with our experimental setup is very difficult; the major problem arises in separating primary[35] and secondary[38] contributions from underlying Si layers.

In another LEED study, evidence for a disordered (5×2) structure has been observed from annealed Au submonolayers on Si(111).[75] This was not seen in our work. However, the (5×2) features could arise from the multiplicity of bridge sites within a surface (1×1) unit cell. For example, adjacent Au atoms within the rows of the proposed models (Figs. 6 and 7) could occupy two different kinds of bridge sites, resulting in a doubling of the (5×1) cell dimension to make it (5×2). The observed LEED pattern[75] may result from coexistence of (5×1) and (5×2) regions.

Finally, it should be noted from Table I that in proceeding from the (1×1) (Au as-deposited) to the (5×1) (annealed) Au-covered surface, there were relatively large increases in the coherent fraction, but small changes in the coherent position for all of the reflections. This suggests that the (1×1) surface involves the same types of adsorption sites as the (5×1) surface, but with considerable disorder.[10]

VI. CONCLUSIONS

Standing-wave measurements of an annealed 0.35-ML Au-covered Si(111) surface, which exhibited a (5×1) reconstruction, have identified unusual Au adsorption sites. The most favorable adsorption site is one embedded in the substrate bridging two second-layer Si atoms, 0.15 Å above the (111) diffraction plane (regardless of the stacking of the first Si layer). More intuitive models involving Au atoms taking on the embedded sixfold hollow

sites, or sitting above the surface in onefold- and threefold-coordinated sites, do not agree with the data. The (1×1) surface produced by Au deposition at room temperature can be considered to be a disordered (5×1) surface, with the preferred Au adsorption site being the same for both surfaces.

This paper constitutes a summary of a Ph.D. dissertation by the first author,[76] which, in addition, contains a discussion of the angular behavior of the photoelectron yield when the Bragg-diffraction condition in a perfect crystal is satisfied.[49]

ACKNOWLEDGMENTS

We wish to thank Gary Navrotski for his assistance in performing the measurements. Valuable help was provided by the CHESS technical staff. This research was supported by the U.S. National Science Foundation Grant Nos. DMR-85-16616 (Materials Science Center, Cornell University) and DMR-84-12465 (CHESS). Support from the Semiconductor Research Corporation (SRC) is also acknowledged.

*Present address: National Synchrotron Light Source, Brookhaven National Laboratory, Upton, NY 11973.

[1]For recent reviews, see G. Le Lay, J. Crystal Growth **54**, 551 (1981); Surf. Sci. **132**, 169 (1983); A. Hiraki, Jpn. J. Appl. Phys. **22**, 549 (1983); Surf. Sci. Rep. **3**, 357 (1984); Surf. Sci. **168**, 74 (1986); C. Calandra, O. Bisi, and G. Ottaviani, Surf. Sci. Rep. **4**, 271 (1985).

[2]T. Narusawa, S. Komiya, and A. Hiraki, Appl. Phys. Lett. **22**, 389 (1973).

[3]L. Braicovich, C. M. Garner, P. R. Skeath, C. Y. Su, P. W. Chye, I. Lindau, and W. E. Spicer, Phys. Rev. B **20**, 5131 (1979).

[4]A. Cros, J. Derrien, C. Mouttet, J. P. Gaspard, P. Lambin, and F. Salvan, J. Phys. (Paris) Colloq. **41**, C8-795 (1980).

[5]E. Bauer and H. Poppa, Thin Solid Films **12**, 167 (1972).

[6]P. Perfetti, S. Nannarone, F. Patella, C. Quaresima, M. Capozi, A. Savoia, and G. Ottaviani, Phys. Rev. B **26**, 1125 (1982).

[7]L. Calliari, M. Sancrotti, and L. Braicovich, Phys. Rev. B **30**, 4885 (1984).

[8]J. J. Lander, Surf. Sci. **1**, 125 (1964).

[9]H. E. Bishop and J. C. Rivière, Brit. J. Appl. Phys. (J. Phys. D) **2**, 1635 (1969).

[10]G. Le Lay and J. P. Faurier, Surf. Sci. **69**, 295 (1977).

[11]N. Osakabe, Y. Tanishiro, K. Yagi, and G. Honjo, Surf. Sci. **97**, 393 (1980).

[12]M. Ichikawa, T. Doi, and K. Hayakawa, Surf. Sci. **159**, 133 (1985).

[13]Y. Yabuuchi, F. Shoji, K. Oura, and T. Hanawa, Surf. Sci. **131**, L412 (1983).

[14]K. Oura, M. Katayama, F. Shoji, and T. Hanawa, Phys. Rev. Lett. **55**, 1486 (1985).

[15]F. Salvan, H. Fuchs, A. Baratoff, and G. Binnig, Surf. Sci. **162**, 634 (1985); A. Baratoff, G. Binnig, H. Fuchs, F. Salvan, and E. Stoll, *ibid.* **168**, 734 (1986).

[16]S. M. Durbin, L. E. Berman, B. W. Batterman, and J. M. Blakely, J. Vac. Sci. Technol. A **3**, 973 (1985); Phys. Rev. B **33**, 4402 (1986).

[17]B. W. Batterman, Phys. Rev. **133**, A759 (1964).

[18]B. W. Batterman, Phys. Rev. Lett. **22**, 703 (1969).

[19]M. von Laue, Ann. Phys. (Leipzig) **23**, 705 (1935).

[20]B. W. Batterman and H. Cole, Rev. Mod. Phys. **36**, 681 (1964).

[21]S. K. Andersen, J. A. Golovchenko, and G. Mair, Phys. Rev. Lett. **37**, 1141 (1976).

[22]M. V. Kruglov, E. A. Sozontov, V. N. Shchemelev, and B. G. Zakharov, Kristallografiya **22**, 693 (1977) [Sov. Phys.—Crystallogr. **22**, 397 (1977)].

[23]A. M. Afanas'ev and V. G. Kon, Zh. Eksp. Teor. Fiz. **74**, 300 (1978) [Sov. Phys.—JETP **47**, 154 (1978)].

[24]M. V. Kruglov, V. N. Shchemelev, and G. G. Kareva, Phys. Status Solidi A **46**, 343 (1978).

[25]P. L. Cowan, J. A. Golovchenko, and M. F. Robbins, Phys. Rev. Lett. **44**, 1680 (1980).

[26]J. A. Golovchenko, J. R. Patel, D. R. Kaplan, P. L. Cowan, and M. J. Bedzyk, Phys. Rev. Lett. **49**, 560 (1982).

[27]G. Materlik, A. Frahm, and M. J. Bedzyk, Phys. Rev. Lett. **52**, 441 (1984).

[28]K. Akimoto, T. Ishikawa, T. Takahashi, and S. Kikuta, Nucl. Instrum. Methods Phys. Res., Sect. A **246**, 751 (1986).

[29]B. N. Dev, G. Materlik, R. L. Johnson, W. Kranz, and P. Funke, Surf. Sci. **178**, 1 (1986); B. N. Dev, G. Materlik, F. Grey, R. L. Johnson, and M. Clausnitzer, Phys. Rev. Lett. **57**, 3058 (1986).

[30]M. Hart, A. R. D. Rodrigues, and D. P. Siddons, Acta Crystallogr. Sect. A **40**, 502 (1984).

[31]L. E. Berman, S. M. Durbin, and B. W. Batterman, Nucl. Instrum. Methods Phys. Res., Sect. A **241**, 295 (1985).

[32]P. W. Palmberg, J. Vac. Sci. Technol. **12**, 375 (1975).

[33]R. C. Henderson, J. Electrochem. Soc. **119**, 772 (1972).

[34]Y. Ota, Thin Solid Films **106**, 3 (1983).

[35]S. M. Durbin, L. E. Berman, B. W. Batterman, and J. M. Blakely, Phys. Rev. Lett. **56**, 236 (1986).

[36]K. Morizane and P. S. Gleim, J. Appl. Phys. **40**, 4104 (1969).

[37]A. Ishizaka and Y. Shiraki, J. Electrochem. Soc. **133**, 666 (1986).

[38]J. R. Patel, P. E. Freeland, J. A. Golovchenko, A. R. Kortan, D. J. Chadi, and G.-X. Qian, Phys. Rev. Lett. **57**, 3077 (1986).

[39]J. R. Patel, P. E. Freeland, M. S. Hybertsen, D. C. Jacobson, and J. A. Golovchenko, Phys. Rev. Lett. **59**, 2180 (1987).

[40]J. R. Patel, J. A. Golovchenko, P. E. Freeland, and H.-J. Gossman, Phys. Rev. B **36**, 7715 (1987).

[41]1 ML corresponds to 7.83×10^{14} atoms/cm^2 on a Si(111) surface. The coverage was calibrated by comparing the ratio of the Au *NVV* (69 eV) to Si *LVV* (92 eV) Auger peak intensities measured with the CMA with those from samples whose Au coverages were determined using Rutherford-backscattering spectroscopy.

[42]C. G. Darwin, Philos. Mag. (Ser. 6) **27**, 315 (1914); **27**, 675 (1914).

[43]J. A. Prins, Z. Phys. **63**, 477 (1930).

[44]S. Lagomarsino, F. Scarinci, and A. Tucciarone, Phys. Rev. B **29**, 4859 (1984).

[45]M. J. Bedzyk, G. Materlik, and M. V. Kovalchuk, Phys. Rev. B **30**, 2453 (1984).

[46]M. J. Bedzyk and G. Materlik, Phys. Rev. B **32**, 6456 (1985).

[47]If one chooses the bulk unit-cell origin to lie in the diffraction plane, then on the low-angle side of the reflection, $v\rightarrow180°$,

and on the high-angle side, $v \rightarrow 0°$. If absorption is neglected, then the diffraction plane is coincident with the maximum of the real part of the corresponding Fourier component of the electron density. If absorption is not neglected, the diffraction plane is offset from the electron density "symmetry" plane in the $+\mathbf{H}$ direction by a distance proportional to the absorption strength (Ref. 46). For the measurements reported here, this offset is less than 0.2% of a d spacing, which is much smaller than the experimental position error bars.

[48]This condition is usually satisfied when the dipole approximation to the photoelectric absorption cross section is valid, i.e., when the spatial extent of the initial (bound) electron wave function is much smaller than the x-ray wavelength; see H. Wagenfeld, Phys. Rev. **144**, 216 (1966).

[49]If the monitored yield is an angle-resolved photoemission (as in our measurements), then it is not valid to assume that the yield is proportional to the field intensity at the atom center, if the π-polarization geometry is used. An angular anomaly results from interference between the two outgoing photoelectron waves which have azimuthal symmetries about the incident- and diffracted-beam polarization vectors (which are not parallel in the π geometry); in this case, C_1 and C_2 also depend on the angular characters of the initial (bound) and final (free) electron wave functions, as well as on the detector geometry. Nevertheless, the values of these coefficients for the data presented are close to those determined by dynamical theory (i.e., $C_1 = 1$ and $C_2 = \cos 2\theta_B$), due to the extent of angular averaging of the photoelectron yield by the CMA. A standing-wave measurement for which the acceptance solid angle of the CMA was sharply reduced, resulting in C_1 and C_2 values far from the dynamical-theory predictions, will be discussed in another paper; see L. E. Berman and M. J. Bedzyk (unpublished).

[50]N. Hertel, G. Materlik, and J. Zegenhagen, Z. Phys. B **58**, 199 (1985).

[51]B. A. Nesterenko and A. D. Borodkin, Fiz. Tverd. Tela (Leningrad) **12**, 2042 (1970) [Sov. Phys.—Solid State **12**, 1621 (1971)].

[52]The Debye-Waller factor D_H is related to the mean square of the vibrational amplitude $\langle u_H^2 \rangle$ through $D_H = \exp(-2\pi^2 \langle u_H^2 \rangle / d_H^2)$, where d_H is the d spacing (Ref. 45).

[53]M. J. Bedzyk and G. Materlik, Surf. Sci. **152/153**, 10 (1985); Phys. Rev. B **31**, 4110 (1985).

[54]J. Stöhr, R. Jaeger, G. Rossi, T. Kendelewicz, and I. Lindau, Surf. Sci. **134**, 813 (1983).

[55]F. Comin, J. E. Rowe, and P. H. Citrin, Phys. Rev. Lett. **51**, 2402 (1983).

[56]S. A. Chambers, S. B. Anderson, and J. H. Weaver, Phys. Rev. B **32**, 581 (1985).

[57]G. Rossi, D. Chandesris, P. Roubin, and J. Lecante, Phys. Rev. B **34**, 7455 (1986); J. Phys. (Paris) Colloq. **47**, C8-521 (1986).

[58]P. H. Citrin, P. Eisenberger, and J. E. Rowe, Phys. Rev. Lett. **48**, 802 (1982).

[59]P. H. Citrin, J. E. Rowe, and P. Eisenberger, Phys. Rev. B **28**, 2299 (1983).

[60]P. R. Bevington, *Data Reduction and Error Analysis for the Physical Sciences* (McGraw-Hill, New York, 1969), p. 81.

[61]K. N. Tu, Appl. Phys. Lett. **27**, 221 (1975).

[62]F. Houzay, G. M. Guichar, A. Cros, F. Salvan, R. Pinchaux, and J. Derrien, J. Phys. C **15**, 7065 (1982); Physica **117&118B**, 840 (1983).

[63]L. J. Brillson, A. D. Katnani, M. Kelly, and G. Margaritondo, J. Vac. Sci. Technol. A **2**, 551 (1984).

[64]S. A. Chambers, T. R. Greenlee, G. A. Howell, and J. H. Weaver, J. Vac. Sci. Technol. A **3**, 1291 (1985).

[65]H. Dallaporta and A. Cros, Surf. Sci. **178**, 64 (1986).

[66]J. Kanasaki, N. Itoh, and N. Matsunami, Appl. Phys. Lett. **51**, 1072 (1987).

[67]A. Hiraki, J. Electrochem. Soc. **127**, 2662 (1980).

[68]K. Okuno, T. Ito, M. Iwami, and A. Hiraki, Solid State Commun. **34**, 493 (1980).

[69]T. Narusawa, K. Kinoshita, W. M. Gibson, and A. Hiraki, J. Vac. Sci. Technol. **18**, 872 (1981); T. Narusawa, W. M. Gibson, and A. Hiraki, Phys. Rev. B **24**, 4835 (1981).

[70]An adsorption model similar to Hiraki's has recently been proposed; see M. Iwami, T. Terada, H. Tochihara, M. Kubota, and Y. Murata, Surf. Sci. **194**, 115 (1988).

[71]*Handbook of Chemistry and Physics*, 53rd ed., edited by R. C. Weast (Chemical Rubber Co., Cleveland, 1972), p. D-65.

[72]P. A. Bennett, L. C. Feldman, Y. Kuk, E. G. McRae, and J. E. Rowe, Phys. Rev. B **28**, 3656 (1983).

[73]K. Takayanagi, Y. Tanishiro, M. Takahashi, and S. Takahashi, J. Vac. Sci. Technol. A **3**, 1502 (1985); K. Takayanagi, Y. Tanishiro, S. Takahashi, and M. Takahashi, Surf. Sci. **164**, 367 (1985).

[74]Scanning-tunneling-microscopy images have not shown evidence for the survival of the (7×7) surface stacking fault following deposition of Au (Ref. 15) or other metals; see R. J. Wilson and S. Chiang, Phys. Rev. Lett. **58**, 369 (1987); *ibid.* **58**, 2575 (1987); E. J. van Loenen, J. E. Demuth, R. M. Tromp, and R. J. Hamers, *ibid.* **58**, 373 (1987); J. Nogami, S. Park, and C. F. Quate, Phys. Rev. B **36**, 6221 (1987); R. S. Becker, B. S. Swartzentruber, J. S. Vickers, M. S. Hybertsen, and S. G. Louie, Phys. Rev. Lett. **60**, 116 (1988).

[75]H. Lipson and K. E. Singer, J. Phys. C **7**, 12 (1974).

[76]L. E. Berman, Ph.D. dissertation, Cornell University, 1988 (available from University Microfilms, Ann Arbor, MI).